JACC: CARDIOVASCULAR IMAGING
VOL. 10, NO. 6, 2017

ISSN 1936-878X/$36.00
PUBLISHED BY ELSEVIER
http://dx.doi.org/10.1016/j.jcmg.2016.07.005

Noninvasive CT-Derived FFR Based on Structural and Fluid Analysis

A Comparison With Invasive FFR for Detection of Functionally Significant Stenosis

Brian S. Ko, MBBS (Hons), PhD,[a] James D. Cameron, MBBS, BE, MD,[a] Ravi K. Munnur, MBBS,[a] Dennis T.L. Wong, MBBS (Hons), PhD,[a] Yasuko Fujisawa, BSci,[b] Takuya Sakaguchi, PhD,[b] Kenji Hirohata, PhD,[c] Jacqui Hislop-Jambrich, PhD,[d] Shinichiro Fujimoto, MD, PhD,[e] Kazuhisa Takamura, MD, PhD,[e] Marcus Crossett, BSc,[a,f] Michael Leung, MBBS (Hons), PhD,[a] Ahilan Kuganesan, BSc,[a,f] Yuvaraj Malaiapan, MBBS,[a] Arthur Nasis, MBBS (Hons), PhD,[a] John Troupis, MBBS,[a,f] Ian T. Meredith, MBBS (Hons), PhD,[a] Sujith K. Seneviratne, MBBS[a]

ABSTRACT

OBJECTIVES This study describes the feasibility and accuracy of a novel computed tomography (CT) fractional flow reserve (FFR) technique based on alternative boundary conditions.

BACKGROUND Techniques used to compute FFR based on images acquired from coronary computed tomography angiography (CTA) are described. Boundary conditions were typically determined by allometric scaling laws and assumptions regarding microvascular resistance. Alternatively, boundary conditions can be derived from the structural deformation of coronary lumen and aorta, although its accuracy remains unknown.

METHODS Forty-two patients (78 vessels) in a single institution prospectively underwent 320-detector coronary CTA and FFR. Deformation of coronary cross-sectional lumen and aorta, computed from coronary CTA images acquired over diastole, was used to determine the boundary conditions based on hierarchical Bayes modeling. CT-FFR was derived using a reduced order model performed using a standard desktop computer and dedicated software. First, 12 patients (20 vessels) formed the derivation cohort to determine optimal CT-FFR threshold with which to detect functional stenosis, defined as FFR of ≤0.8, which was validated in the subsequent 30 patients (58 vessels).

RESULTS Derivation cohort results demonstrated optimal threshold for CT-FFR was 0.8 with 67% sensitivity and 91% specificity. In the validation cohort, CT-FFR was successfully computed in 56 of 58 vessels (97%). Compared with coronary CTA, CT-FFR at ≤0.8 demonstrated a higher specificity (87% vs. 74%, respectively) and positive predictive value (74% vs. 60%, respectively), with comparable sensitivity (78% vs. 79%, respectively), negative predictive value (89% vs. 88%, respectively), and accuracy (area under the curve: 0.88 vs. 0.77, respectively; $p = 0.22$). Based on Bland-Altman analysis, mean intraobserver and interobserver variability values for CT-FFR were, respectively, -0.02 ± 0.05 (95% limits of agreement: −0.12 to 0.08) and 0.03 ± 0.06 (95% limits: 0.07 to 0.19). Mean time per patient for CT-FFR analysis was 27.07 ± 7.54 min.

CONCLUSIONS CT-FFR based on alternative boundary conditions and reduced-order fluid model is feasible, highly reproducible, and may be accurate in detecting FFR ≤ 0.8. It requires a short processing time and can be completed at point-of-care. Further validation is required in large prospective multicenter settings.
(J Am Coll Cardiol Img 2017;10:663–73) © 2017 by the American College of Cardiology Foundation.

From the [a]Monash Cardiovascular Research Centre, MonashHEART, Department of Medicine, Monash Medical Centre, Monash Health, and Monash University, Melbourne, Victoria, Australia; [b]Toshiba Medical Systems Corporation, Otawara, Japan; [c]Toshiba Corporation, Kawasaki, Japan; [d]Toshiba Medical Australia, North Ryde, Australia; [e]Department of Cardiovascular Medicine, Juntendo University Graduate School of Medicine, Tokyo, Japan; and the [f]Department of Diagnostic Imaging, Monash Medical Centre, Monash Health, Melbourne, Clayton, Victoria, Australia. Drs. Ko and Wong are funded by the National

JACC: CARDIOVASCULAR IMAGING, VOL. 10, NO. 6, 2017
JUNE 2017:663–73

ABBREVIATIONS AND ACRONYMS

CFD = computational fluid dynamics

CT = computed tomography

CTA = computed tomography angiography

CT-FFR = computed tomography fractional flow reserve

FFR = fractional flow reserve

ICA = invasive coronary angiography

IDI = integrated discrimination improvement index

NRI = net reclassification index

Ischemia assessment remains the cornerstone management of stable coronary artery disease (CAD), as its presence and burden determine outcomes and benefits from revascularization (1). Traditional stress tests and imaging modalities provide assessment of overall ischemic burden, yet remain limited in ischemia localization and guiding revascularization on a per-vessel basis. Invasive fractional flow reserve (FFR) is the established standard for assessing the functional significance of coronary stenosis. It represents the distal coronary-to-aortic pressure ratio and leads to improved clinical outcomes when used to guide revascularization, compared to invasive angiography (1,2).

The technique of FFR_{CT} (HeartFlow, Redwood City, California) is used to noninvasively derive invasive FFR by applying the principles of computational fluid dynamics (CFD) and image-based modeling from typically acquired coronary computed tomography angiography (CTA) images, which permit computation of coronary flow and pressures along the length of the entire coronary tree. Compared with invasive FFR, the diagnostic accuracy of FFR_{CT} ranges between 73% and 81% and has a sensitivity of 86% to 93% and a specificity of 54% to 79% (3,4), and its comparative cost effectiveness has been described previously (5,6).

SEE PAGE 674

In CFD-based techniques, pressure and flow along the coronary tree are derived using 3 broad steps (7), as follows: 1) generation of an anatomical model using computed tomography (CT) data; 2) application of mathematical principles to derive coronary boundary conditions; and 3) use of a numerical solution which accounts for fluid dynamics to simulate flow and pressure.

In FFR_{CT}, the boundary conditions are determined by allometric scaling laws and assumptions regarding coronary microvascular resistance (7), and the numerical solution used to simulate fluid dynamics permits 3-dimensional (3D) pressure and flow evaluation in each pixel of the coronary tree.

In this paper, we describe a novel technique (CT-FFR) in which boundary conditions are derived by accounting for the structural deformation changes in the coronary lumen and adjacent aorta across the entire diastolic phase of the cardiac cycle (8,9). The numerical solution used to simulate fluid dynamics in CT-FFR is a reduced-order (1-dimensional) fluid model which permits evaluation of pressure and flow at each luminal cross-section of the coronary tree (10).

Phantom feasibility studies using a pump connected to flexible tubes with various degrees of stenosis have demonstrated excellent correlation between CT-FFR and invasive FFR measurements (8,9). However the feasibility and diagnostic performance of CT-FFR in human populations and its incremental value compared with that of coronary CTA remain unknown. Our primary aim was to determine the feasibility and diagnostic accuracy of CT-FFR to detect functionally significant stenosis. Our secondary aim was to evaluate the incremental value of CT-FFR in coronary CTA. Fractional flow reserve was used as the reference standard.

METHODS

Symptomatic patients with no known CAD who were at intermediate or high risk (11) and were scheduled for clinically mandated elective invasive coronary angiography (ICA) at Monash Medical Centre were screened. Exclusion criteria included <40 years of age, atrial fibrillation, renal insufficiency (estimated glomerular filtration rate <60 ml/min/1.73 m^2), bronchospastic lung disease requiring long-term steroid therapy, morbid obesity (body mass index ≥40 kg/m^2) and contraindications to iodinated contrast. Screened patients were included in the study upon providing consent to undergo a research-indicated coronary CTA and invasive FFR in at least 1 major epicardial vessel with >2-mm diameter during invasive coronary angiography. Among the 42 patients who were recruited in the study, the first 12 patients formed the derivation cohort, and the subsequent 30 patients formed the validation cohort. The study was approved by the institutional human research ethics committee, and all participants gave written informed consent.

Heart Foundation of Australia and Robertson Family Scholarship. Dr. Wong is funded by the National Health and Medical Research Council of Australia. Dr. Ko has been an invited speaker at symposiums sponsored by St. Jude Medical, Pfizer, Bristol-Myers Squibb, and Eli Lilly. Ms. Fujisawa, Mr. Sakaguchi, and Dr. Hislop-Jambrich are employees of Toshiba Medical Systems Corp. Dr. Hirohata is an employee of Toshiba Corp. Dr. Meredith has received honoraria for serving on strategic advisory boards of Boston Scientific and Medtronic. Dr. Seneviratne has been an invited speaker at a Toshiba sponsored meeting. All other authors have reported that they have no relationships relevant to the contents of this paper to disclose.

Manuscript received March 21, 2016; revised manuscript received July 11, 2016, accepted July 14, 2016.

COMPUTED TOMOGRAPHY IMAGING PROTOCOL. Patients underwent cardiac CT assessment using a 320-row detector CT scanner (Aquilion One Vision; Toshiba Medical Systems Corp., Tokyo, Japan). The CT protocol consisted of calcium score followed by coronary CTA. All patients received sublingual nitroglycerine, and additional beta-blockers were administered to achieve a pre-scan heart rate of <60 beats/min in accordance with Society of Cardiovascular Computed Tomography guidelines (12). Scanning was triggered in the arterial phase, using automated contrast bolus tracking in a region of interest placed in the descending aorta, and automatically triggered at 300 Hounsfield units. Scan parameters for coronary CTA were: detector collimation: 320 × 0.5 mm; tube current: 300 to 500 mA; tube voltage: 100 to 120 kV; gantry rotation time: 270 ms; and temporal resolution: 135 ms. Prospective electrocardiogram gating was used, covering 70% to 99% of the R-R interval. Effective radiation dose was calculated by multiplying the dose-length product by a constant (k = 0.014 mSv/mGy/cm) (13).

CORONARY CTA ANALYSIS. Stenosis severity on coronary CTA was interpreted using a dedicated workstation (Vitrea Fx 6, Vital Images, Minnetonka, Minnesota) by 2 experienced CT angiographers (S.F., K.T.) at the Juntendo coronary CTA core laboratory, blinded to the results of ICA and FFR in accordance with the 18 coronary segment model (14); disagreement was resolved by consensus. A vessel was considered significant if there was ≥1 segment which was nonevaluable or showed >50% luminal stenosis.

CT-FFR ANALYSIS. The CT-FFR analysis was performed by 2 experienced post-processing technicians (Y.F., T.S.) at the Toshiba Medical Systems Corp. core laboratory, blinded to the results of the invasive FFR, using a standard desktop computer (Xeon E5-2620, 6 core × 2 processor, Intel, Mountain View, California) and dedicated software (Toshiba Medical Systems Corp.) (**Figure 1**). 3D models of the coronary tree were constructed from CT slice data using the FC03 reconstruction kernel (SurePlaque, Toshiba Medical Systems Corp.). Vessel centerline and luminal contours were automatically processed. Manual adjustments were performed as required.

Four CT images were reconstructed from the available phases (at 70%, 80%, 90%, and 99% of R-R interval). Each millimeter of the coronary tree from the vessel inlet to outlet (up to 1.8 mm in diameter) was registered and permitted calculation of structural

FIGURE 1 CT-FFR Methodology

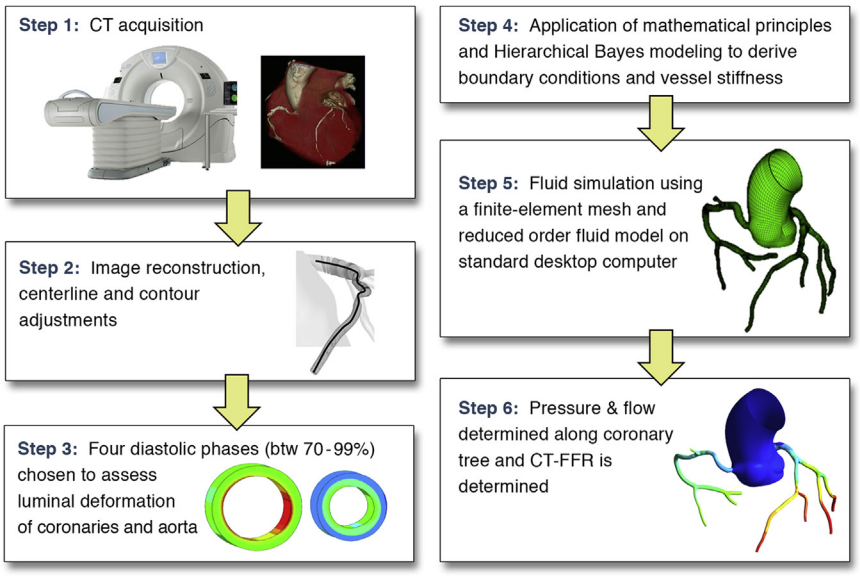

An anatomical luminal model was reconstructed from coronary CTA (Steps 1 and 2). Boundary conditions were determined by assessment of luminal deformation of coronary arteries and aorta during diastole and hierarchical Bayes modeling (Steps 3 and 4). Fluid simulation was based on a reduced-order model using a standard desktop computer. Pressure, flow, and CT-FFR were determined along the coronary tree (Steps 5 and 6). CTA = computed tomography angiography; CT-FFR = computed tomography fractional flow reserve.

TABLE 1 Patient Characteristics (N = 30)

Age, yrs	
Mean ± SD (N)	60.0 ± 8.5 (30)
Median	60
Minimum–maximum	43.0–80.0
Sex	
Males	70.0 (21/30)
Females	30.0 (9/30)
Diabetes mellitus	30.0 (9/30)
Hypertension*	73.3 (22/30)
Hyperlipidemia†	80.0 (24/30)
Smoking	
Former smokers	33.3 (10/30)
Current smokers	26.7 (8/30)
Never smoked	40.0 (12/30)
Prior myocardial infarction	0.0 (0/51)
Angina type*	
Typical	13.3 (4/30)
Atypical	66.7 (20/30)
Noncardiac chest pain	20.0 (6/30)
Updated Diamond-Forrester risk score	
Intermediate (20%–80%) pre-test risk	86.7 (30)
Body mass index	
Mean ± SD (N)	28.5 ± 4.6 (30)
Median	29
Creatinine, mmol/l	
Mean ± SD (N)	79.1 ± 16.2 (30)
Median	80.5

Values are % (n/N) or % (n) unless otherwise indicated. *Blood pressure >140/90 mm Hg or treatment for hypertension. †Total cholesterol >180 mg/dl or treatment for hypercholesterolemia.

data including the cross-sectional luminal deformation, volume variation in the vessels and aortic root. Blood was modeled as a non-Newtonian fluid using the Herschel-Bulkley fluid constitutive model.

A number of physical principles and relationships were used to derive the boundary conditions, as follows: 1) the volume variation in the aorta is related to inlet coronary flow rate during diastole (70% to 100%); 2) the boundary pressures of the coronary outlets during diastole relate to the cross-sectional luminal deformation, vessel stiffness, cross-sectional luminal shape, and the pressure at which flow rate was 0; 3) the extent of pressure loss between the aorta and coronary artery outlets relates to the flow rate of the coronary outlets; and 4) microvascular resistance is minimized during diastole and constant such that pressure is proportional to flow (15).

TABLE 2 Vessel Characteristics (N = 30 Patients; N = 58 Vessels)

Calcium score, Agatston units	
Mean ± SD (N)	910.3 ± 1,075.6 (30)
Median	528
Patients with coronary CTA maximum stenosis >50%	50.0 (15/30)
Vessels with coronary CTA maximum stenosis >50%	43.1 (25/58)
Patients with QCA maximum stenosis >50%	53.3 (16/30)
Vessels with QCA maximum stenosis on >50%	29.3 (17/58)
Patients with CT-FFR ≤0.80	48.3 (14/29)
Vessels with CT-FFR ≤0.80	33.9 (19/56)
Patients with FFR ≤0.80	46.7 (14/30)
Vessels with FFR ≤0.80	33.0 (19/58)
Patients with FFR ≤0.80 in >1 vessel	10.0 (3/30)

Values are % (n/N) unless otherwise indicated.
CTA = computed tomography angiography; CT-FFR = computed tomography fractional flow reserve; QCA = quantitative coronary angiography.

TABLE 3 CT Scan Acquisition Characteristics (N = 30)

Heart rate prior to coronary CTA (beats/min)	
Mean ± SD (N)	52.5 ± 6.8 (30)
Median	52.0
Nitrates administered	100.0 (30/30)
Beta blockers administered	90.0 (27/30)
Radiation calculated from DLP, mSv	
Mean ± SD (N)	4.9 ± 2.2 (30)
Median	4.7
kV	
100	46.7 (14/30)
120	53.3 (16/30)
mA	
Mean ± SD (N)	630.3 ± 157.8
Minimum, maximum	340, 820
Single beat acquisition	100 (30/30)

Values are % (n/N) unless otherwise indicated.
DLP = dose-length product.

Hierarchical Bayes modeling was used to integrate CT data and structural and fluid analysis conditions. This model takes into account the probability distribution based on observed structural measurements and prior data; the latter is generated using simulation-based parameter surveys and Markov chain Monte Carlo simulation.

Based on the finite element mesh model reconstructed from the CT data, structural and fluid analyses were performed using the finite difference method based on the continuity, momentum, and constitutive equations. A reduced-order fluid model was used with a fluid resistance database which provided 1-dimensional pressure and flow simulations across the coronary tree. The clinical site provided the Toshiba core laboratory, with the distance measured from the vessel ostium to the pressure sensor of FFR wire for each interrogated vessel, in order to directly match the FFR result with CT-FFR estimate. CT-FFR values were calculated from the derived pressures along the length of the vessel to a minimum diameter width of 1.8 mm.

INVASIVE ANGIOGRAPHY AND FFR. Invasive coronary angiography was performed according to standard practice, either through the femoral or the radial approach. FFR was performed during ICA in at least 1 vessel with diameter ≥2 mm and 10% to 90% visual stenosis and was chosen at the discretion of the operator, blinded to the CT findings. The pressure wire (Certus 7, St. Jude Medical, St. Paul, Minnesota) was calibrated and electronically equalized with the aortic pressure before being placed in the distal third of the coronary artery being interrogated. Intracoronary glyceryl trinitrate (100 μm) was injected to minimize vasospasm. Intravenous adenosine was administered (140 μm/kg per min) through an intravenous line in the antecubital fossa. At steady-state hyperemia, FFR was recorded and calculated by dividing the mean coronary pressure measured with the pressure sensor placed distally to the stenosis by the mean aortic pressure measured through the guide catheter. The pressure sensor was then pulled back into the tip of the guiding catheter, and only runs with ≤0.03 drift were accepted for analysis. A FFR value of ≤0.80 was chosen to define functionally significant stenosis (1).

QUANTITATIVE CORONARY ANGIOGRAPHY. Quantitative coronary angiography was performed using an 18-segment coronary model (14). This was performed using a semiautomated edge detection system (Xcelera Cath R3.2, Philips, Amsterdam, the Netherlands) by 2 experienced cardiologists (Y.M., M.L.) at the Monash Heart core laboratory who were blinded to FFR and CT findings, with disagreement resolved by consensus. Each coronary segment was visually assessed for degree of luminal stenosis, and a vessel was considered significant if there was ≥1 segment which was nonevaluable or showed >50% luminal stenosis.

STATISTICAL ANALYSIS. Continuous variables are mean ± SD if normally distributed. Categorical variables are frequencies (percentages). Sensitivity, specificity, positive predictive value (PPV) and NPV were calculated to predict the ability of each modality to identify functionally significant stenoses on a per-vessel basis. The association between the studied CT technique and the FFR was assessed using a generalized estimation approach. Patient identity was included as a cluster variable to account for likely within-individual correlations, given that repeated measures were made from each individual. FFR as a dichotomous variable was assumed to have a binomial probability distribution. Interobserver and intraobserver reproducibility were performed on 16 randomly selected vessels. Receiver-operating characteristic curve (ROC) area under the curve analysis was undertaken to evaluate the discriminatory ability of coronary CTA and CT-FFR to detect FFR ≤0.8. The optimal CT-FFR threshold established

FIGURE 2 Correlation Between CT-FFR and Invasive FFR

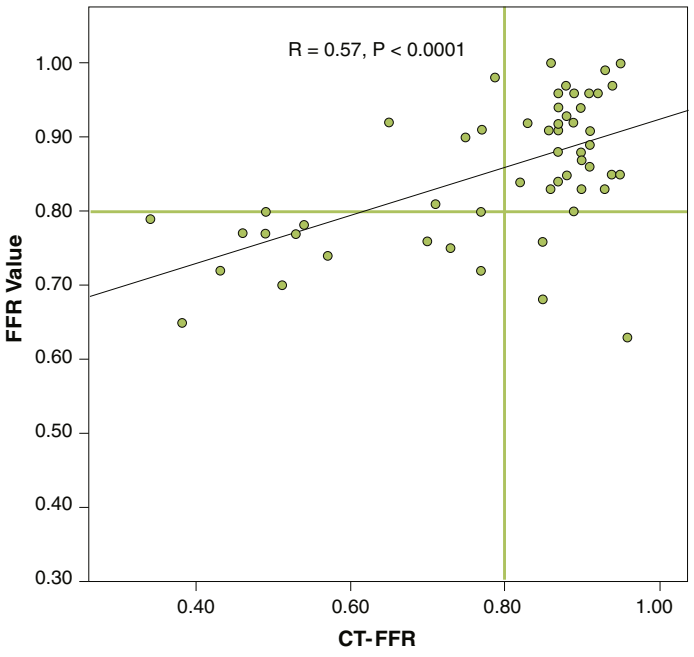

Abbreviations as in Figure 1.

FIGURE 3 Bland-Altman Plot of CT-FFR and Invasive FFR

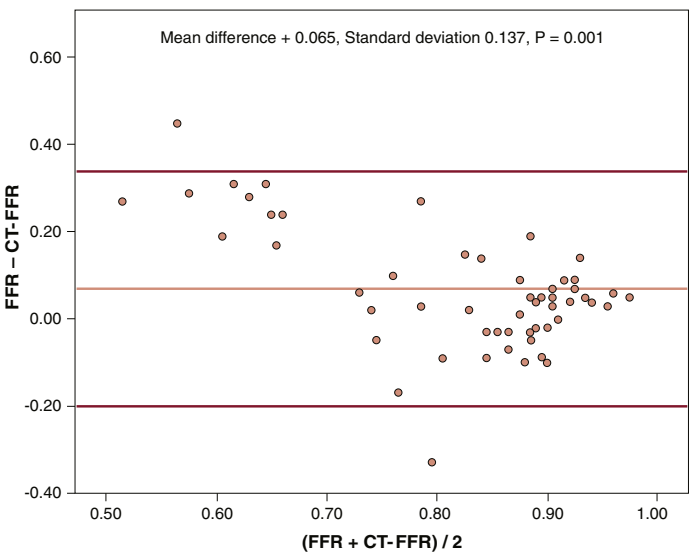

Abbreviations as in Figure 1.

JACC: CARDIOVASCULAR IMAGING, VOL. 10, NO. 6, 2017
JUNE 2017:663–73

TABLE 4 Per Vessel Diagnostic Accuracy of Coronary CT, CT-FFR, Quantitative and Invasive Coronary Angiography Compared With FFR

	Coronary CTA (≥50%) (n = 58)	CT-FFR (≤0.80) (n = 56)	QCA (≥50%) (n = 58)	Visual ICA (≥50%) (n = 58)
True positive	15	14	9	17
True negative	29	33	31	21
False positive	10	5	8	18
False negative	4	4	10	2
% Accuracy	77.6	83.9	69.0	65.5
% Sensitivity	78.9 (53.9–93.0)	77.8 (51.9–92.6)	47.4 (25.2–70.5)	89.5 (65.5–98.2)
% Specificity	74.3 (57.6–86.4)	86.8 (71.1–95.1)	79.5 (63.1–90.1)	53.8 (37.4–69.6)
% PPV	60.0 (38.9–78.2)	73.7 (48.6–89.9)	52.9 (28.5–76.1)	48.6 (31.7–65.7)
% NPV	87.9 (70.9–96.0)	89.2 (73.6–95.6)	75.6 (59.4–87.1)	91.3 (70.5–98.5)
AUC	0.77 (0.65–0.88)	0.88 (0.76–1.0)	0.67 (0.51–0.83)	0.82 (0.71–0.94)

Values are n, %, or % (95% confidence interval).
AUC = area under the curve; ICA = invasive coronary angiography; NPV = negative predictive value; PPV = positive predictive value; other abbreviations as in Table 1.

in the derivation cohort, which provided at least 65% sensitivity and maximized the sum of sensitivity and specificity, was chosen as the threshold for the validation cohort. Areas under the ROC curves were compared using the approach of DeLong et al. (16) with a Bonferroni adjustment for pair-wise comparisons. The incremental value of CT-FFR to coronary CTA in discriminating significant FFR was assessed by 2 methods. The integrated discrimination improvement (IDI) index and the category-free net reclassification index (NRI) were used to determine whether CT-FFR improved vessel classification as hemodynamically significant compared with coronary CTA alone (17). An IDI index that is significantly >0 is taken to demonstrate the incremental value of the studied technique when added to coronary CTA. The NRI can be calculated by consideration of the sum of 2 separate components, vessels with FFR ≤0.8 and vessels with FFR >0.8. For vessels with FFR ≤0.8, we assigned 1 for upward reclassification, −1 for downward reclassification, and 0 for vessels which did not change their risk

FIGURE 4 ROC of CT-FFR in the Derivation Cohort and Coronary CTA and CT-FFR in the Validation Cohort, in Predicting FFR Significant Stenosis

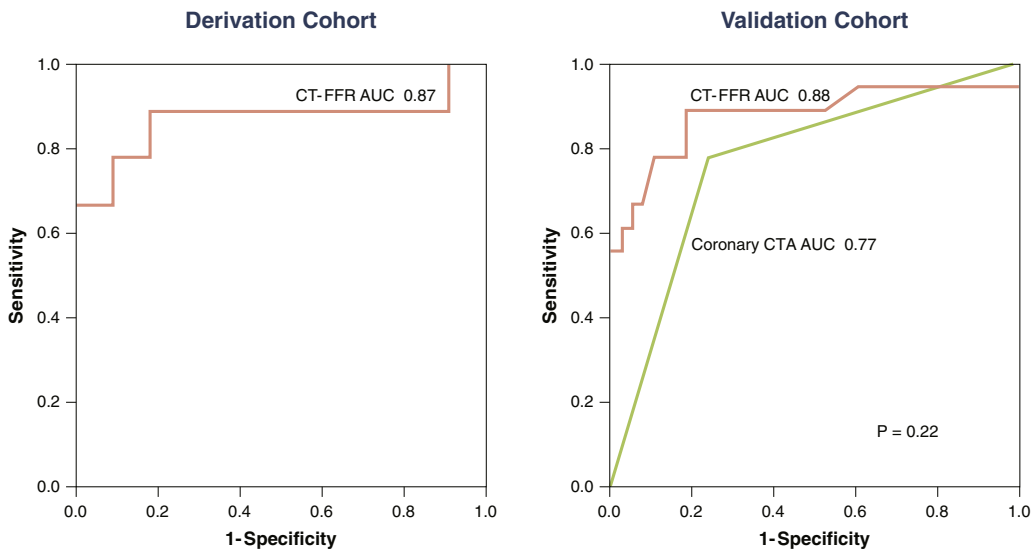

ROC = receiver operating characteristic curve; other abbreviations as in Figure 1.

FIGURE 5 Representative Case Example From Study

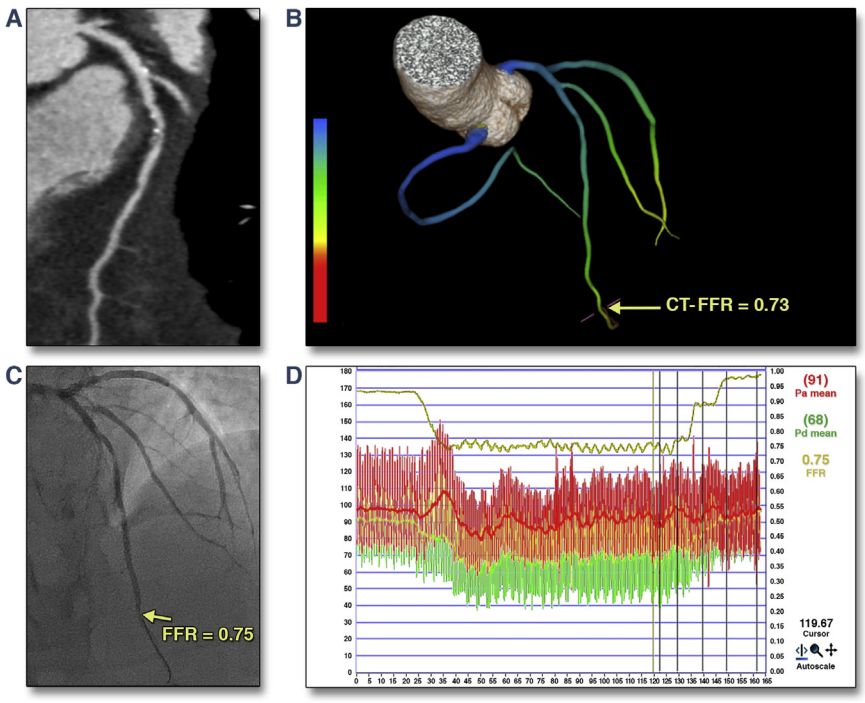

A 53-year-old man with intermediate risk of coronary artery disease presented with chest pains. Coronary CTA demonstrated a moderate (51% to 70%) stenosis in the mid LAD **(A)**. The CT-FFR was 0.73 in the distal LAD **(B)**. Invasive coronary angiography again demonstrated a moderate stenosis in the mid LAD **(C)**; fractional flow reserve was 0.75 in the distal LAD. LAD = left anterior descending artery; other abbreviations as in Figure 1.

category by applying CT-FFR compared with coronary CTA alone. For vessels with FFR >0.80, the opposite was performed. The sum of the individual scores was divided by the number of vessels in each group. Intraobserver and interobserver variability in assessment of CT-FFR were determined using Bland-Altman analysis. Statistical analysis was performed using SPSS version 20 (SPSS, Chicago, Illinois) and STATA version 13.1 (STATA Corp., College Station, Texas) software. A p value <0.05 was considered statistically significant.

RESULTS

In the derivation cohort, 12 patients, including 20 vessels, were retrospectively studied. A CT-FFR threshold ≤0.8 provided optimal sum of sensitivity and specificity. The ROC area under the curve (AUC) using this threshold was 0.87 (95% confidence interval [CI]: 0.68 to 1.00), with a sensitivity of 66.7% and a specificity of 90.9%.

In the validation cohort, 34 consecutive patients with suspected CAD underwent 320-detector coronary CTA and ICA, using FFR measurement at Monash Medical Centre (n = 34) between July 2014 and January 2016 (Table 1). Four patients were excluded due to inaccurate FFR assessment (n = 1), inability to perform CT assessment due to deviation from image acquisition protocol (n = 1), intramyocardial bridging (n = 1), and poor image quality (n = 1). Finally, 58 vessels were analyzed from 30 patients.

Mean age was 60 years old, and 70% were male. Of the 58 coronary arteries, 24 were left anterior descending (LAD), 2 were diagonal branches, 20 were left circumflex arteries (LCx) or marginal branches, 2 were ramus branches, and 10 were right coronary arteries (RCA). Baseline patient and vessel characteristics are listed in Tables 1 and 2. CT scan parameters are listed in Table 3. The number (percentage) of vessels with FFR ≤0.80 was 19 (33%).

RELATIONSHIP BETWEEN CT-FFR AND FFR. CT-FFR was successfully computed in 56 of 58 vessels (97%).

FIGURE 6 Representative Case Example From the Study

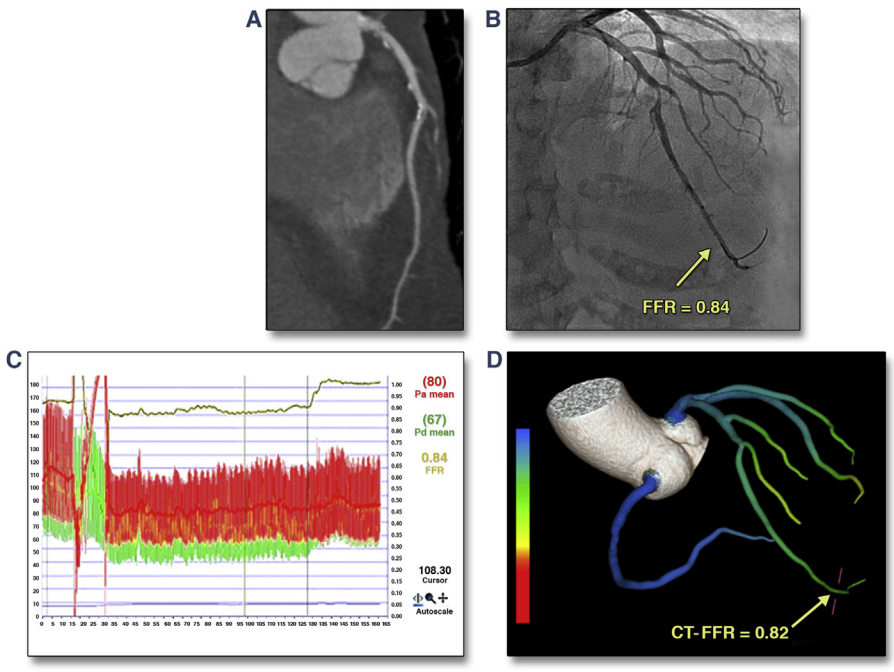

A 66-year-old woman with intermediate risk of coronary artery disease presented with atypical chest pains. Coronary CTA demonstrated a moderate (51% to 70%) stenosis in the mid LAD after the second diagonal bifurcation **(A)**. Invasive coronary angiography demonstrated the stenosis was severe at 70% **(B)**. Fractional flow reserve in the distal LAD was 0.84 **(C)**. CT-FFR, performed blinded to the FFR result, was 0.82 **(D)**. Abbreviations as in Figures 1 and 5.

The CT data in 1 patient (including 2 vessels) was corrupted and precluded analysis. CT-FFR was significantly lower in vessels with hemodynamically significant stenoses than in vessels without hemodynamically significant stenosis (0.63 vs. 0.87, respectively; $p < 0.0001$). Figure 2 illustrates the correlation between CT-FFR and invasive FFR. CT-FFR demonstrated a statistically significant yet modest correlation with invasive FFR (Pearson $R = 0.57$; $p < 0.0001$). On Bland-Altman analysis, there was good agreement between FFR and CT-FFR, with a difference of 0.065 ± 0.137 (95% CI: −0.20 to 0.33) (Figure 3).

DIAGNOSTIC PERFORMANCE OF CORONARY CTA AND CT-FFR. The performance of coronary CTA and of CT-FFR for diagnosis of hemodynamically significant stenosis are summarized in Table 4 and Figure 4. Two cases of correlation are provided as examples in Figures 5 and 6. The ROC analysis for coronary CTA alone showed an AUC of 0.77 ($p = 0.001$). Sensitivity, specificity, PPV, and NPV were 78.9%, 74.3%, 60%, and 87.9%, respectively. Four hemodynamically significant stenoses (3 LAD, 1 LCx, FFR range 0.68 to 0.78) were identified as <50% stenotic on coronary CTA.

The ROC curve analysis for CT-FFR demonstrated an AUC of 0.88 ($p < 0.001$) by using a CT-FFR threshold of ≤0.80, which was comparable with that for coronary CTA ($p = 0.22$). This resulted in 14 true positives, 33 true negatives, 5 false positives (1 in LAD, 2 in LCx, 2 in RCA), and 4 false negatives (2 in LAD, 1 in LCx, 1 in RCA). Sensitivity, specificity, PPV, and NPV of CT-FFR were 78%, 87%, 74%, and 89%, respectively. The net reclassification index for CT-FFR compared with coronary CTA was 1.29 (SE: 0.29; $p < 0.0001$). The integrated discrimination improvement for CT-FFR was 0.21 with SE of 0.06 ($p = 0.0002$).

TIME TAKEN AND REPRODUCIBILITY OF CT-FFR ANALYSIS. The mean per-patient time required for CT-FFR analysis was 27.07 ± 7.54 min. There was a mean intraobserver variability of -0.02 ± 0.05, and the 95% limits of agreement were −0.12 to 0.08. The mean interobserver variability was 0.03 ± 0.06 (95% limits of agreement: −0.07 to 0.19).

TABLE 5 Comparison of FFR_{CT} and CT-FFR

	HeartFlow FFR_{CT}	Toshiba CT-FFR
Scan characteristics		
Scanner requirements	≥64-detector CT	320-detector CT
Scan acquisition	Prospective ECG gating	Prospective ECG gating
Phases required	One phase (typically 75% of R-R interval)	4 phases between 70% and 100% (typically 70%, 80%, 90%, 99% of R-R interval)
Requirements for nitrates and heart rate control	Compulsory	Compulsory
CT anatomical model		
How is it generated?	Semiautomated using dedicated software, with manual adjustments	Semiautomated using SurePlaque software (Toshiba Medical Systems Corp.), with manual adjustments as required
Mathematical model		
Derivation of boundary outlet conditions	1) Boundary outlet pressure and resistance are derived from diameter of coronary outlets and myocardium subtended (allometric scaling laws) 2) Assumptions are made regarding microvascular resistance—assumed to be 0.24 of microvascular resistance at rest	1) Boundary outlet pressure is derived from the changes in luminal CSA, vessel stiffness vessel shape and flow at rate 0 2) Pressure difference from aorta to coronary outlet determines outlet coronary flow 3) Assumption is made that resistance is constant such that pressure is proportional to flow
Derivation of boundary inlet conditions	1) Brachial pressure is used to derive aortic pressure 2) Total coronary inlet flow is proportional to the total amount of myocardium subtended	1) Common blood pressure is used to derive aortic pressure 2) Coronary inlet flow during diastole is proportional to the change in aortic volume at the same time
Fluid assumptions	Blood modeled as Newtonian fluid	Blood modeled as non-Newtonian fluid
Numerical solution to account for fluid dynamics		
How is it computed?	1) Using a finite element mesh model derived from CT data 2) 3 Dimensional fluid model of coronary arteries generated to estimate flow and pressure at each pixel of coronary tree	1) Using a finite element mesh model derived from CT data 2) Reduced order (1D) fluid model of the coronary outlets generated to estimate flow and pressure at each luminal cross-section of the coronary tree.
Practical considerations		
Operator	Processed by a technician at HeartFlow laboratory	Feasible by radiographer or physician at point-of-care
Computational requirements	Parallel supercomputer required for computing the fluid analysis model	Standard desktop computer
Time	1–4 h	30 min

1D = 1-dimensional; ECG = electrocardiography; FFR_{CT} = technique used to noninvasively derive invasive FFR.

DISCUSSION

In this prospective study, we demonstrated the feasibility and high diagnostic accuracy of a novel CT-based technique, CT-FFR, to assess the functional significance of coronary stenosis as determined by invasive fractional flow reserve. Compared with coronary CTA alone, our results demonstrate CT-FFR provides superior specificity and positive predictive value, while sensitivity, negative predictive, and accuracy are comparable. CT-FFR also provided incremental benefit compared with that of coronary CTA alone. The lack of difference in overall accuracy as represented by the ROC AUC may be attributed to an underpowered sample size.

CT-based techniques to derive noninvasive FFR require 3 broad steps: 1) generation of an anatomical model based on CT data; 2) application of mathematical principles to derive boundary inlet and outlet conditions which represent cardiac output, aortic pressures, outlet coronary flow and pressure and microvascular resistance; and 3) performance of a fluid simulation using identified boundary conditions to derive flow and pressures along the entire coronary tree. The differences in methodology between CT-FFR and HeartFlow FFR_{CT} are highlighted in Table 5. They differ primarily in the mathematical principles in which boundary conditions are derived and the fluid model in which coronary flow and pressure are simulated. In FFR_{CT}, form and function relationships of arteries and the myocardium were used to derive boundary conditions. Typically, the technique only requires 1 CT acquisition phase (e.g., at 75% of R-R interval) during diastole. In

CT-FFR, conditions of boundary outlet and inlet pressure are derived from determining the change in cross-sectional area of coronary vessels and aorta across the entire diastole. This information is obtained using 4 phases of CT acquisition, typically at 70%, 80%, 90%, and 99% of the R-R interval.

The ideal coronary CTA-based CFD technique is one which permits accurate and timely functional assessment of coronary stenosis. The numerical solution to simulate fluid dynamics for FFR_{CT} is one which is based on a 3D fluid model, which permits pressure and flow estimation for each point or pixel along the coronary tree. This rigorous process is aimed at providing added information and accuracy, although it requires a prolonged processing time and the use of a supercomputer at the HeartFlow laboratory in Redwood City, California. For this reason, the technique currently requires a turnover time of 24 h, which includes the need for offsite image transfer and an image processing time of 1 to 4 h depending on disease burden and CT image quality (4). In CT-FFR, fluid simulation is based on a reduced-order (1-dimensional) model (9,18), which permits assessment of pressure and flow at each luminal cross-section of the coronary tree. The theoretical concern is that this may reduce diagnostic performance compared with the 3D model. This report demonstrates the promise of CT-FFR, which was found to have a high diagnostic accuracy despite the use of the reduced-order fluid model, comparable with that reported for other resting coronary CTA-based CFD techniques (18,19). The advantages offered by this model are the much reduced processing time and the ability to derive this information without the use of a supercomputer. Our results demonstrate the feasibility to process CT-FFR in <30 min, using standard desktop computers, which permits point-of-care CT-FFR calculation. Notably, our results demonstrate excellent reproducibility, with little interobserver and intraobserver variability on repeated measures.

STUDY LIMITATIONS. The study has a number of inherent limitations. It is a single-center study with a small sample of subjects and vessels. Accordingly, it is not powered to detect AUC differences compared with those of coronary CTA alone, as such numerical comparisons with previous CFD-based CT studies should be interpreted cautiously. Larger multicenter, well powered prospective studies are required to further establish the diagnostic performance of CT-FFR. For the same reason, subanalyses of intermediate, major subbranch or calcified lesions will be underpowered and only hypothesis-generating. The population studied consisted of patients awaiting elective ICA, hence the potential for selection bias. Patients who had previously undergone revascularization or had had myocardial infarction were excluded from the study; for that reason, the accuracy of CT-FFR in these populations remains unknown. All scans were performed using 320-detector CT, and the feasibility of this technique applied to narrow detector CT is not known. Finally, the influence of heart rate, motion, and calcification, which may affect image quality and impact diagnostic performance, was not evaluated in this study.

CONCLUSIONS

Noninvasive FFR based on structural and fluid analysis using a reduced-order flow model is a highly reproducible technique. These pilot data suggest that FFR may provide accurate detection of functionally significant coronary stenosis and can be processed over <30 min. Larger multicenter prospective studies are required to further establish its diagnostic performance and incremental value compared with coronary CTA.

ACKNOWLEDGMENTS The authors acknowledge Mr. Shigeo Kaminaga for advice on study design, Mr. Norikazu Yamada for contribution to assessment of the reproducibility of CT-FFR, Ms. Nozomi Masubuchi for work as a member of the core laboratory staff, Dr. Mitsuaki Kato and Mr. Akira Kano for work related to CT-FFR algorithm optimization, Dr. Rich Mather for technical support, and Ms. Chloe Steveson for support in scan protocol.

ADDRESS FOR CORRESPONDENCE: Dr. Brian S. Ko, Monash Heart, Monash Cardiovascular Research Centre, 246 Clayton Road, Clayton, 3168 VIC, Australia. E-mail: brian.ko@monashhealth.org.

PERSPECTIVES

COMPETENCY IN MEDICAL KNOWLEDGE: Noninvasive CT-FFR using boundary conditions determined by assessing coronary luminal and aortic deformation during diastole and a reduced-order fluid model is feasible, highly reproducible and may be accurate in detecting FFR ≤0.8. It requires a short processing time and can be completed at point-of-care.

TRANSLATIONAL OUTLOOK: The diagnostic performance of CT-FFR requires further evaluation and validation in large prospective multicenter observational studies.

REFERENCES

1. Tonino PA, De Bruyne B, Pijls NH, et al. Fractional flow reserve versus angiography for guiding percutaneous coronary intervention. N Engl J Med 2009;360:213–24.

2. De Bruyne B, Fearon WF, Pijls NH, et al. Fractional flow reserve-guided PCI for stable coronary artery disease. N Engl J Med 2014;371:1208–17.

3. Min JK, Leipsic J, Pencina MJ, et al. Diagnostic accuracy of fractional flow reserve from anatomic CT angiography. JAMA 2012;308:1237–45.

4. Norgaard BL, Leipsic J, Gaur S, et al. Diagnostic performance of non-invasive fractional flow reserve derived from coronary CT angiography in suspected coronary artery disease: the NXT trial. J Am Coll Cardiol 2014;63:1145–55.

5. Douglas PS, Pontone G, Hlatky MA, et al. Clinical outcomes of fractional flow reserve by computed tomographic angiography-guided diagnostic strategies vs. usual care in patients with suspected coronary artery disease: the prospective longitudinal trial of FFRct: outcome and resource impacts study. Eur Heart J 2015;36:3359–67.

6. Hlatky MA, De Bruyne B, Pontone G, et al. Quality-of-life and economic outcomes of assessing fractional flow reserve with computed tomography angiography: PLATFORM. J Am Coll Cardiol 2015;66:2315–23.

7. Taylor CA, Fonte TA, Min JK. Computational fluid dynamics applied to cardiac computed tomography for noninvasive quantification of fractional flow reserve: scientific basis. J Am Coll Cardiol 2013;61:2233–41.

8. Hirohata K, Kano A, Goryu A, et al. A novel CT-FFR method for the coronary artery based on 4D-CT image analysis and structural fluid analysis. SPIE Medical Imaging 2015;9412-94:26.

9. Kato M, Hirohata K, Kano A, et al. Fast CT-FFR analysis method for the coronary artery based on 4D-CT image analysis and structural and fluid analysis. Proceedings of the American Society of Mechanical Engineers 2015 International Mechanical Engineering Congress and Exposition. New York, NY: ASME, 2015:51124.

10. Coenen A, Lubbers MM, Kurata A, et al. Fractional flow reserve computed from noninvasive CT angiography data: diagnostic performance of an on-site clinician-operated computational fluid dynamics algorithm. Radiology 2015;274:674–83.

11. Gibbons RJ, Chatterjee K, Daley J, et al. ACC/AHA/ACP-ASIM guidelines for the management of patients with chronic stable angina: executive summary and recommendations. A report of the American College of Cardiology/American Heart Association Task Force on Practice Guidelines (Committee on Management of Patients with Chronic Stable Angina). J Am Coll Cardiol 1999;33:2092–197.

12. Raff GL, Chinnaiyan KM, Cury RC, et al. SCCT guidelines on the use of coronary computed tomographic angiography for patients presenting with acute chest pain to the emergency department: a report of the Society of Cardiovascular Computed Tomography Guidelines Committee. J Cardiovasc Comput Tomogr 2014;8:254–71.

13. Hausleiter J, Meyer T, Hermann F, et al. Estimated radiation dose associated with cardiac CT angiography. JAMA 2009;301:500–7.

14. Raff GL, Abidov A, Achenbach S, et al. SCCT guidelines for the interpretation and reporting of coronary computed tomographic angiography. J Cardiovasc Comput Tomogr 2009;3:122–36.

15. Sen S, Escaned J, Malik IS, et al. Development and validation of a new adenosine-independent index of stenosis severity from coronary wave-intensity analysis: results of the ADVISE (ADenosine Vasodilator Independent Stenosis Evaluation) study. J Am Coll Cardiol 2012;59:1392–402.

16. Delong ML, Duncan BD, Parker JH. Parametric extension of the classical exposure-schedule theory for angle-multiplexed photorefractive recording over wide angles. Appl Opt 1998;37:3015–30.

17. Pencina MJ, D'Agostino RB Sr., D'Agostino RB Jr., Vasan RS. Evaluating the added predictive ability of a new marker: from area under the ROC curve to reclassification and beyond. Stat Med 2008;27:157–72; discussion 207–12.

18. Coenen A, Lubbers MM, Kurata A, et al. Coronary CT angiography derived fractional flow reserve: methodology and evaluation of a point of care algorithm. J Cardiovasc Comput Tomogr 2016;10:105–13.

19. Koo BK, Erglis A, Doh JH, et al. Diagnosis of ischemia-causing coronary stenoses by noninvasive fractional flow reserve computed from coronary computed tomographic angiograms. Results from the prospective multicenter DISCOVER-FLOW (Diagnosis of Ischemia-Causing Stenoses Obtained Via Noninvasive Fractional Flow Reserve) study. J Am Coll Cardiol 2011;58:1989–97.

KEY WORDS computed tomography, coronary disease, fractional flow reserve, imaging, ischemia, quantitative coronary angiography